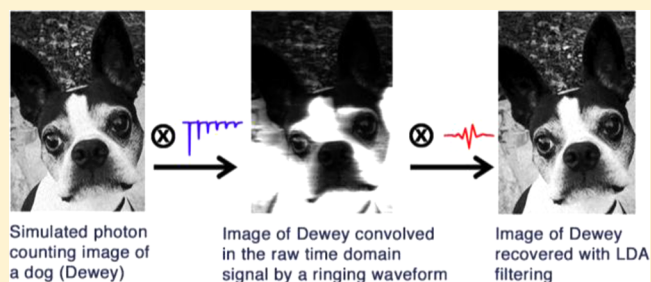# Digital Deconvolution Filter Derived from Linear Discriminant Analysis and Application for Multiphoton Fluorescence Microscopy

Shane Z. Sullivan, Paul D. Schmitt, Ryan D. Muir, Emma L. DeWalt, and Garth J. Simpson*

Department of Chemistry, Purdue University, 560 Oval Drive, West Lafayette, Indiana 47907, United States

ABSTRACT: A digital filter derived from linear discriminant analysis (LDA) is developed for recovering impulse responses in photon counting from a high speed photodetector (rise time of ~1 ns) and applied to remove ringing distortions from impedance mismatch in multiphoton fluorescence microscopy. Training of the digital filter was achieved by defining temporally coincident and noncoincident transients and identifying the projection within filter-space that best separated the two classes. Once trained, data analysis by digital filtering can be performed quickly. Assessment of the reliability of the approach was performed through comparisons of simulated voltage transients, in which the ground truth results were known *a priori*. The LDA filter was also found to recover deconvolved impulses for single photon counting from highly distorted ringing waveforms from an impedance mismatched photomultiplier tube. The LDA filter was successful in removing these ringing distortions from two-photon excited fluorescence micrographs and through data simulations was found to extend the dynamic range of photon counting by approximately 3 orders of magnitude through minimization of detector paralysis.

Simulated photon counting image of a dog (Dewey)

Image of Dewey convolved in the raw time domain signal by a ringing waveform

Image of Dewey recovered with LDA filtering

Photon, ion, and particle counting can offer substantial signal-to-noise (S/N) improvements in the detection of weak signals by removing thermal electronic noise, baseline drift, and noise from variation in detector gain. In the simplest application, photon counting (n.b., this same analysis also applies to ion and particle counting) is performed using a discriminator, in which a count is recorded for each transient exceeding the discriminator threshold. The upper limit on the dynamic range in photon counting is dictated by bunching of photons in time, often described as "paralysis". Bunching can introduce two sources of measurement bias. First, two or more time-coincident photons will still only produce a single count as measured by a discriminator. Second, the temporal response function of the detector and electronics imposes a time delay for the voltage to recover below the discriminator threshold before an additional count can be recorded.

The first problem of undercounting from time-coincident multiple-photon events has been explored in several previous studies. In single-threshold measurements, it has been shown by several investigators that the bias can be removed by analyzing the raw measurements in terms of binomial counting statistics, given that the discriminator has only two possible outcomes for each laser pulse (no photons are present, or one or more photons are present). The binomially distributed measurements can then be related back to the Poisson distribution to determine the underlying mean of the Poisson, which is proportional to the unbiased detected intensity. In recent studies by Kissick et al., an analytical expression was derived for the uncertainty in the Poisson mean obtained by binomial counting and used to interpret second harmonic generation (SHG) measurements generated from a pulsed

laser.[1] On the basis of these analytical expressions, Muir et al. subsequently demonstrated a method of stitching counting and signal averaging in SHG microscopy measurements for real-time S/N optimization.[2] However, these results are strictly limited to pulsed excitation measurements, in which the time delay between laser pulses is significantly longer than the instrument response time.

The second source of bias from paralysis is from multiple noncoincident photons falling within the finite rise/fall time of the detector and electronics (i.e., the impulse response function), such that the voltage does not recover below the discriminator threshold prior to the next photon detection event. The detection of discrete events with a sensor can be mathematically modeled as a convolution of instantaneous impulses with the impulse response function, where the temporal locations of all the underlying impulses are the parameters of interest.

Several strategies have been adopted to correct for this second and routinely more insidious source of bias. A common solution is to reduce the signal level or to use a series of detectors that detect fractions of the total light intensity to diminish the occurrence of paralysis,[3,4] though diminishing the observed signal necessarily diminishes the S/N of the measurement. Other strategies disable signal observation for a period of time after a successful count to wait out the temporal response function, though this typically leads to under-estimation of the true number of counts and limits the speed

of acquisition.[5] The use of multiple detectors, or single multiplexed detectors, can reduce effects of paralysis and increases data acquisition times.[5−7] However, each detector adds its own dark current and allows for modest gains in dynamic range (doubling the number of detectors doubles the noise from dark counts and yields only a factor of 2 increase in dynamic range).

Alternative approaches rely on correcting for dead-time and "pulse pile-up" using analytical models and fitting of experimental signal outputs, which are computationally expensive and typically too time-consuming to be performed in real-time for fast (>MHz count rates) counting applications.[4,8−14] The simplest strategies based on nonlinear curve-fitting, such as are routinely done in spectroscopy and chromatography, require initial selection of guess values and multiple iterations to achieve convergence and are not guaranteed to avoid false minima. However, the greatest limitation of nonlinear curve fitting is arguably the time required to perform the analysis. With streaming data rates corresponding to a new data point every 12.5 ns at the repetition rate of a conventional ultrafast laser, real-time fitting for a single channel of data is well beyond the current capabilities of curve-fitting algorithms. More recently, digital processing of the time-dependent output was shown to lead to increased analysis speed for real-time analysis for X-ray photon counting, made possible by the use of simple algorithms coupled with relatively long-lived voltage transients (10s to 100s of ns).[15−18]

Deconvolution of the raw input prior to threshold based counting has been pursued to a much lesser degree. The measured transient results from a convolution of the initial photon absorption event with the impulse response function of the detector/instrument. If the detector output were a simple impulse, rather than a rising and falling transient, there would be no dead-time issues related to overlapping transients.[12] For data initially stored in digital form, deconvolution can in principle be performed simply by digital filtering with a filter function representing the inverse of the impulse response function (often calculated in the Fourier domain). However, in practice, this simple approach tends to greatly amplify the noise, often overwhelming relatively weak signals. The noise-amplification problem can be minimized by using a Wiener filter (or a variant thereof), but these standard approaches often suffer from difficulties in handling noise in general, require prior knowledge of a noise-free impulse response, and are specifically optimized for normally distributed noise. As a result, the robustness of the existing techniques is arguably limited in scope.

In the present work, an alternative approach for deconvolution is proposed and evaluated on the basis of digital filters derived from LDA. This approach is based on maximizing the resolution between time-coincident and noncoincident events. Simulations of the impulse response were performed to assess the scope of use of the algorithm. The signal and noise are integrated into the LDA training sets, such that the filters are inherently optimized to include the impact of the filter on both. Measurements performed using a set of photomultiplier tubes for optical detection of continuous wave sources were performed to test experimentally. A complex impulse response function was observed and successfully deconvolved. Although a specific example is provided for photon counting, the proposed LDA-based digital filtering may serve as a general approach for deconvolution in other applications as well.

■ THEORETICAL FOUNDATION

Digital filters are widely used in signal processing in either the time or space domain. In the present work, digital filtering was performed in the time domain (depicted in Figure 1). Digital
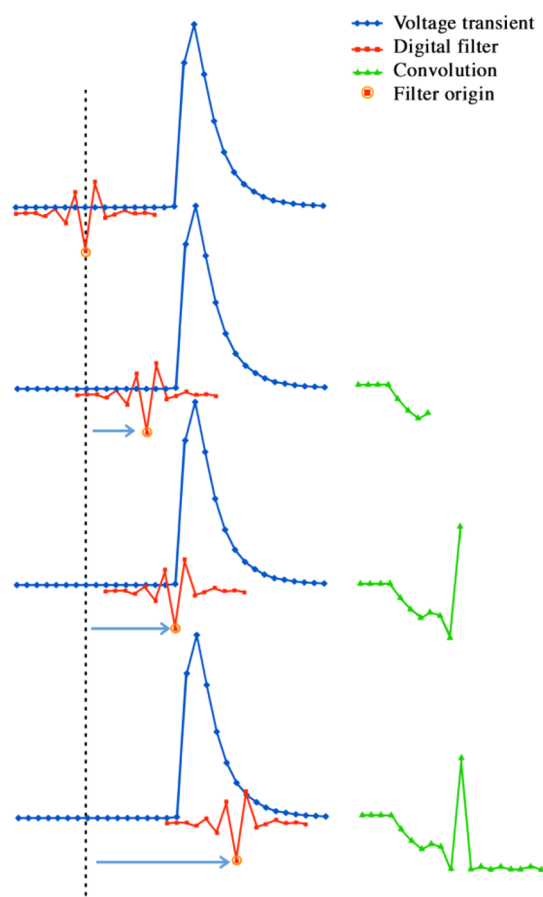

Figure 1. Graphical depiction of the process of digital filtering through convolution of the filter and the signal. The digital filter (red) is translated across the signal trace (blue). The dot product of the filter and signal replaces the data point in the signal trace that corresponds to the filter origin (indicated by the arrows), generating the filtered signal (green).

filtering involves a transformation of a signal (blue trace in Figure 1) through convolution with a digital filter (red trace). As the filter is translated across the signal, the filtered trace is generated (green trace).

The digital filter design proposed in this work targets recovery of a temporally sharp impulse for an arbitrary detector impulse response function using a digital filter constructed on the basis of LDA. LDA is a supervised approach for separating high-dimensional data into distinct classes. In the present application for digital filtering, the length of the filter, L, defines the dimensionality of the space. Two classes are defined for separation: (i) one class in which the voltage transients are time-coincident with the center of the filter and (ii) another in which they are noncoincident, either preceding or following by random time-steps. The coincident training set is generated from numerous independent measurements of the single-photon response function (e.g., obtained from the dark counts), with each measurement corresponding to a single point in the L-dimensional space of the filter. The noncoincident set was generated by randomly time-shifting either the same or a new
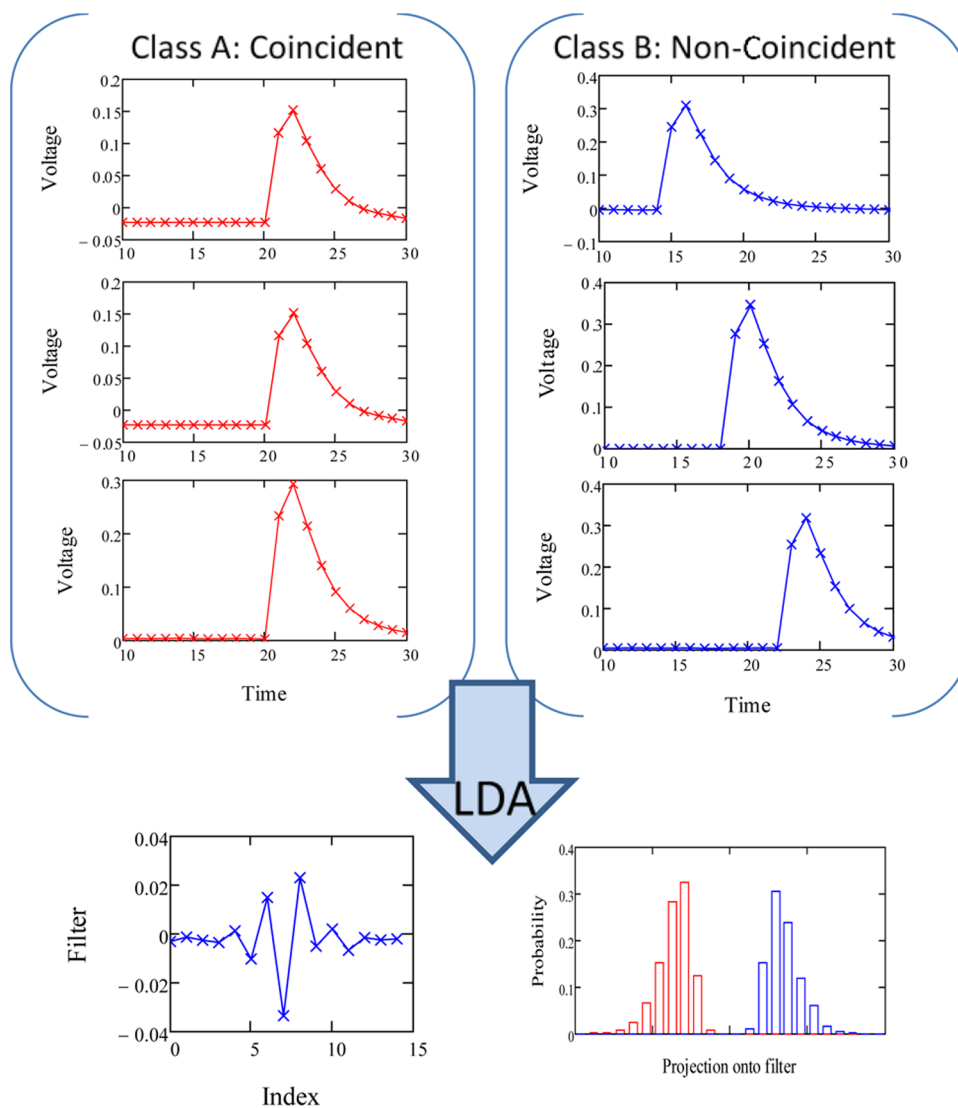
Figure 2. Temporally coincident and noncoincident signals (Top). After linear discriminant analysis, a digital filter is constructed, along with projections of the temporally coincident and noncoincident signals.

coincident data set. An example of this process for simulated data is shown in Figure 2. Defining the classes in this manner maximized the resolution between transients initiated at the filter origin and all other closely neighboring and temporally overlapping transients. Formally, it is not the resolution itself that is maximized but rather the closely related value of the Fisher linear discriminant J, given by eq 1 for a two-class system.

$$J(\vec{w}) = \frac{(\mu_c - \mu_n)^2}{s_c^2 + s_n^2} \tag{1}$$

In eq 1, J is a constant evaluated for a particular direction $\vec{w}$ within the L-dimensional space of the filter (i.e., a particular selection of elements). The parameters μ_c and μ_n correspond to the average projected values of the coincident and non-coincident classes, respectively, along the direction $\vec{w}$. The variance matrix in the coincident class S_c is given by eq 2, in which N_c is the number of coincident waveforms used in the training set, $\mathbf{V}_{c_i}$ is the ith time-dependent coincident single-photon response, and $\overline{\mathbf{V}_c}$ is the mean waveform.

$$S_c = \frac{1}{N_c} \sum_{i=1}^{N_c} (\mathbf{V}_{c_i} - \overline{\mathbf{V}_c})(\mathbf{V}_{c_i} - \overline{\mathbf{V}_c})^T \tag{2}$$

The length L of the waveform spans the temporal range of the single-photon voltage transient. Using an analogous definition for the variance in the noncoincident class S_n, the total within class variance is given by eq 3.

$$S_w = S_c + S_n \tag{3}$$

The particular unit vector $\vec{w}^*$ that maximizes the Fisher linear discriminant for a two-class system is generated from S_w^{-1}:

$$\vec{w}^* = \frac{S_w^{-1}(\overline{\mathbf{V}_c} - \overline{\mathbf{V}_n})}{|S_w^{-1}(\overline{\mathbf{V}_c} - \overline{\mathbf{V}_n})|} \equiv \mathbf{F} \tag{4}$$

The vector $\vec{w}^*$ directly serves as the filter function $\mathbf{F}$ to be used for digital deconvolution of the raw data.

The Fisher discriminant is remarkably similar to the definition of resolution for two overlapping peaks. Therefore, the vector $\mathbf{F}$ corresponds to the direction in the L-dimensional space of the filter that provides the greatest experimental resolution between the coincident and noncoincident classes.
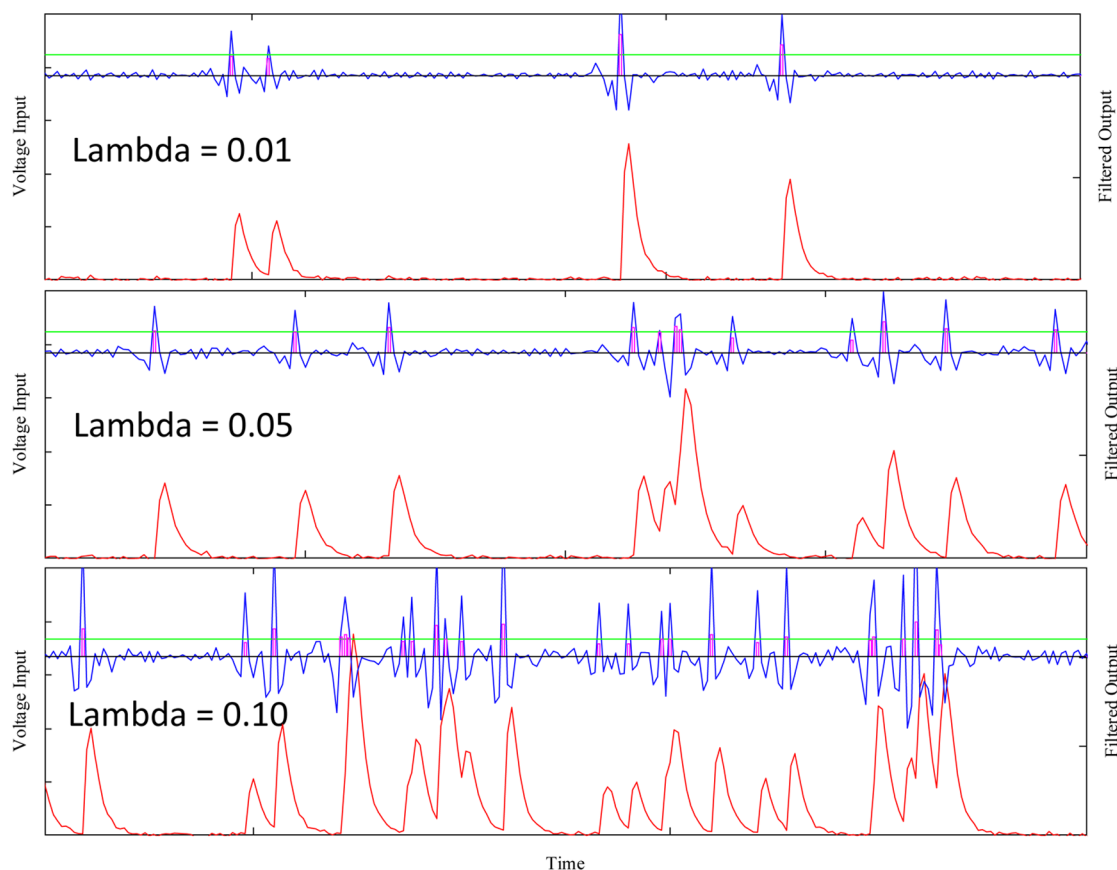
Figure 3. Simulated detector data of three measured intensities. The temporal pulse locations are evident in the raw data (red), though a threshold discrimination technique would not successfully count every pulse. After LDA filtering (blue), a threshold (green) can successfully count every pulse (purple).

When the origin of the filter (typically the center) is time-coincident with the onset of the transient, the scalar output of the filter is given by the dot product of the filter with the transient. Analogously, application of the filter function in a noncoincident position will correspond to a projection of the noncoincident class. Consequently, convolution of the time-trace by the digital filter **F** generated by LDA maximizes the contrast between coincident and noncoincident events to optimally recover deconvolved δ-function single pixel maxima at the location of the transient onsets.

Following digital filtering with the LDA-based filter, photon counting of the recovered impulse responses was performed by counting the number of pixels above a selected threshold in the postfiltered deconvolved time-trace. In practice, high-pass filtering is also subsequently performed prior to counting to remove a rolling low-frequency background introduced by the filter. The rolling features arise as a consequence of the maximization of the resolution between coincident and noncoincident events by LDA, rather than a maximization of the absolute voltage above baseline.

■ METHODS

Simulations with known ground-truth results were performed to assess the performance of LDA-derived digital filtering relative to both conventional photon counting and signal averaging. To produce the training sets, each photon generated a random peak height to model a log-normal distribution in gain in the PMT. A mean μ_L of 7 mV and standard deviation σ_L of 4 mV describing the log-normal distribution were selected

on the basis of measured characteristics for PMTs similar to those used in the present study. The temporal impulse response was also approximated by a log-normal function. For the coincident training set, the initial onset of the pulse was assumed to be at time zero in the center of the filter. The noncoincident training set was generated by offsetting the initial onset by normally distributed random shifts $\Delta\tau$. Each trial also included addition of random $1/f$ noise, generated by Fourier transformation of normally distributed time-trace, multiplication by $(1/(f + b))^{1/2}$, in which f is the frequency and $b = 0.005$ is a constant describing the time-scale for $1/f$ fluctuations, followed by inverse Fourier transformation to recover a time-trace. Qualitatively similar results were observed with normally distributed random noise.

In the simulations of the experimental data acquisition, each time-point contained a Poisson-distributed random number of photons, where λ was the mean of the Poisson distribution (typically less than 1). The time-traces also included $1/f$ noise calculated identically as the simulated data used to generate the training sets.

The probability of two or more photons arriving within a single time-step becomes non-negligible as the mean of the Poisson distribution approaches unity, which can introduce additional bias not accounted for directly by deconvolution alone. The LDA-filtering approach is designed to maximize the separation between transients produced at separations of more than one time-step of the digitizer and will therefore not be able to correct for the recording of a single count from two or more simultaneous photons. Fortunately, this source of bias can be

corrected by connecting the measured counts (distributed according to a binomial distribution, with only two possible outcomes) to the underlying number of photons described by a Poisson distribution. Using algorithms developed previously,[1,19] the mean λ and standard deviation σ_λ of the Poisson distribution in a given Δt time window are given below, where p is the mean probability for successful counting and N is the number of measured time-points used to assess the mean.

$$\lambda = -\ln(1 - p) \qquad (5)$$

$$\sigma_\lambda{}^2 = \frac{p}{N(1 - p)} = \frac{e^\lambda - 1}{N} \qquad (6)$$

For a sufficiently large number of measurements, the experimental mean of p provides a reasonable estimate for the true mean of p, from which the mean and standard deviation of the underlying Poisson distribution can be determined through eqs 5 and 6.

Two-photon excited ultraviolet fluorescence (TPE-UVF) images of pure L-tryptophan crystals (Sigma- Aldrich) were acquired using a custom microscope. Briefly, a Fianium Inc., ultrafast fiber laser (1060 nm, 150 fs, 80 MHz) output was doubled to generate 530 nm, which served as the incident light source for TPE-UVF excitation. The incident beam was scanned along the fast axis using a resonant vibrating mirror (~4 kHz) and along the slow axis using a galvanometer mirror. The scanned beam was directed through an inverted Nikon microscope (TE2000) through telecentric lens pairs and dichroic mirrors and focused onto the sample using a 10× objective (Nikon). TPE-UVF signal generated from the sample was split into its horizontal and vertical components using a Glan-Taylor polarizer, both of which were detected on two separate photomultiplier tubes (PMTs) in the reflected direction. TPE-UVF signal was passed through a filter stack (SP01-532RS-25 and FF01-440/SP-25 filters Semrock) to reject the fundamental 530 nm light and pass two-photon tryptophan emission (~350 nm). The voltage transients from the photomultiplier tubes were flash digitized using oscilloscope cards from AlazarTech (ATS 9462) at 160 MHz, with the laser providing the master clock to the digitizer cards. To artificially produce a noisy ringing transient, the oscilloscope cards were set to an internal impedance of 1 MΩ and the PMT with a nominal impedance of 50 Ω was connected to the oscilloscope cards with a 20 m long cable and a 400 Ω resistor in parallel at the oscilloscope card input. Experimental training sets were acquired from one highly signal averaged waveform generated from the impedance mismatched PMT signal with added normally distributed noise. For the coincident training set, the initial onset of the pulse was assumed to be at time zero in the center of the filter with the noncoincident training set generated by offsetting the initial onset, as described previously for the simulated data.

RESULTS AND DISCUSSION

Simulations were performed to evaluate the characteristics of the filtering approach. Training sets of 6000 coincident and 6000 noncoincident time-traces were used to generate the digital filter shown in Figure 2. Three representative images of each of the training set data are also shown in the figure. The histogram shows the distribution of values for the dot products of the training set time-traces with the coincident digital filter,

demonstrating the degree of resolution between the two classes.

Application of the filter was performed on simulated data representing a sensor exhibiting an exponential decay temporal response function (Figure 3). The temporal location of each pulse is apparent by eye in the simulated raw data, though a threshold counting technique would not be able to successfully count the number of pulses for incidences of significant pulse pileup. After LDA filtering in blue, the temporal location of each pulse is marked by a large positive transient and can be threshold counted as represented by the green threshold and purple count markers.

In this simulated data set, the temporal locations of each pulse are known *a priori*, and the quality of the technique can be assessed as a function of threshold position. The ratio of true positives vs false positives as the threshold is swept across the full range of positive values is shown in Figure 4 as a receiver
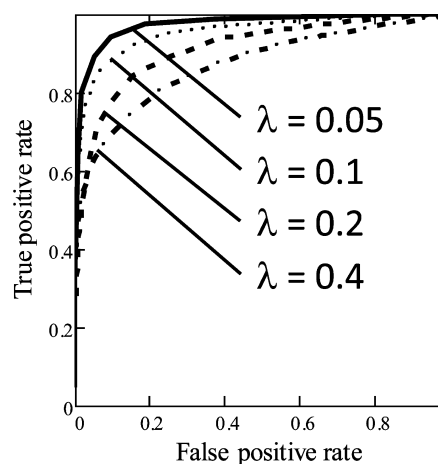

Figure 4. Receiver operating characteristic curve for LDA filtered data. The error rate is relatively low for good threshold settings, even in situations of high pulse pileup ($\lambda = 0.4$).

operating characteristic curve. A data point at the top-left of the graph represents an optimal measurement, with few false positives or false negatives. The drop-off in the true positive rate at higher λ values is consistent with the presence of pulse pileup, though the algorithm still performs well at high intensities in which voltage transients are initiated in almost half the time-points ($\lambda = 0.4$).

EXPERIMENTAL DEMONSTRATION

An experimental impulse response function was chosen to be more challenging than a simple log-normal or exponential decay by inducing substantial ringing in the impulse response. The load on a photomultiplier tube was terminated with a 400 Ω resister in parallel with an internal 1 MΩ resister of the oscilloscope card. By using a long transmission cable (20 m), a series of reflections arose from each transient (Figure 5a). After generation of the LDA filter (Figure 5b) and LDA filtering the data (Figure 5c, green trace), a high-pass filter was applied to adjust the shifted baseline (Figure 5c, blue trace). The temporal location of the initial impulse was the position of the first and largest spike in the raw data, which the LDA analysis marked with a strong positive transient.

The mechanism of action of the digital filter optimized by LDA to recover an impulse response on just the first voltage transient of the ringing waveform may not be immediately
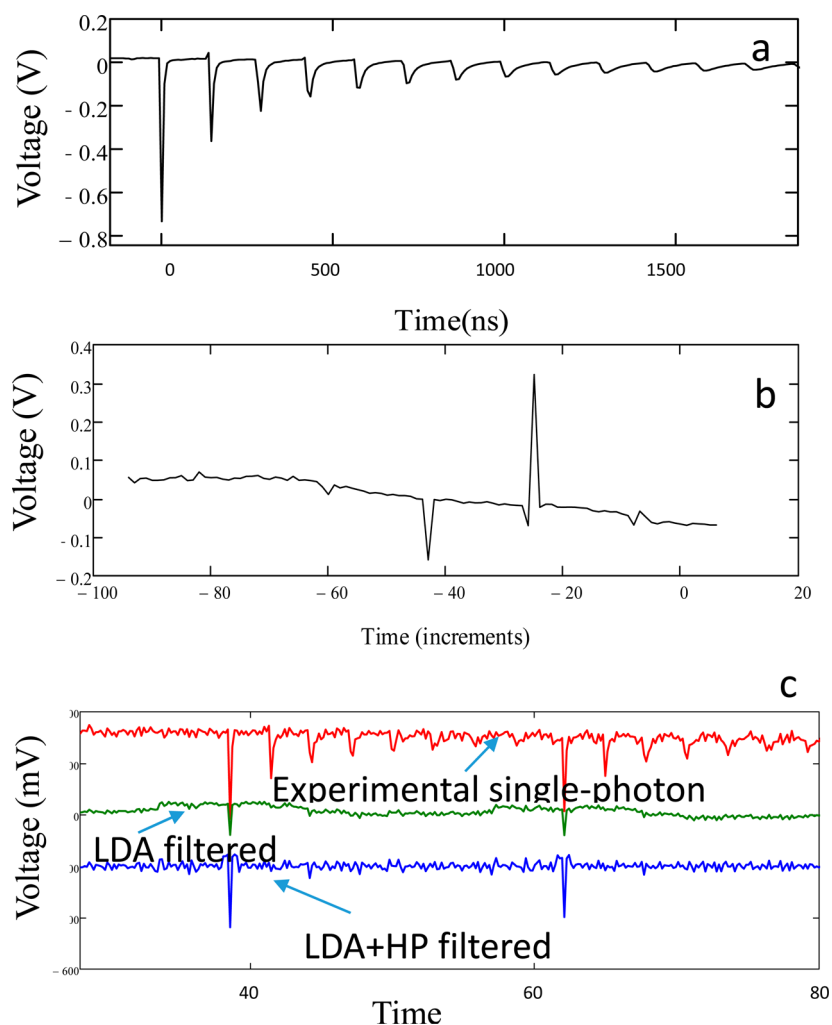
Figure 5. Deconvolution of the experimentally measured waveform with ringing to recover an impulse response; (a) representative waveform produced upon single photon absorption, (b) filter produced by LDA in order to perform the deconvolution, and (c) representative measurements prior to filtering, filtering with the LDA-based filter, and filtering with both an LDA and high-pass (HP) filter.

obvious. However, we conjecture that the digital filter is designed to exploit the nonlinearity in the exponentially decaying peak heights from the multiple transients. If it is assumed that the peak heights in the transient decay linearly with time (a reasonable approximation for the later ringing pulses), then baseline can be recovered by appropriately rescaling and inverting the later peak. In this way, the higher intensity peak and the rescaled lower intensity peak will cancel in the filtered output. Provided the amplitude scales linearly with time, this same strategy removes all the later-time peaks. However, the nonlinearity in the exponential decay results in a greater disparity between the relative peak height of the first transient and the second compared to all the subsequent adjacent peaks. Consequently, convolution with the digital filter retains residual peak height at that position but no others.

The relative count rate (megacounts per second) across multiple optical intensities for various counting algorithms is shown in Figure 6, simulated on the basis of the measured ringing waveform training set as the impulse response function. LDA filtering substantially improved the accuracy of the counts when compared to threshold counting the raw data, which overestimated the counts due to the ringing present in the response function. In addition to over counting, the use of the unfiltered data also introduced errors in the photon arrival
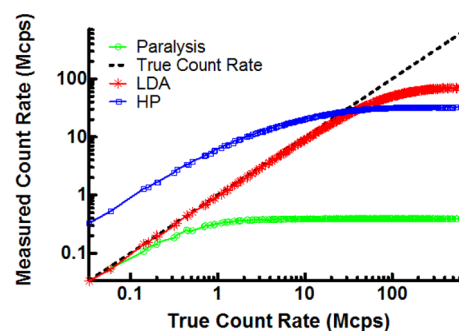

Figure 6. Comparison of different count methods for ringing data. LDA filtering recovered a better estimator for the counting rate compared to counting the raw data (high-pass filter alone) or counting with a timeout (paralysis) for the response function.

times from the recurring pulses. Imposing a dead-time delay to allow the impulse response function to return to baseline (paralysis) recovered the true count rate at low intensities. However, many counts were missed at higher intensities as the probability of photons originating in the dead-time delays became significant. For comparison, application of the same data with the LDA filter extended the linear dynamic range of
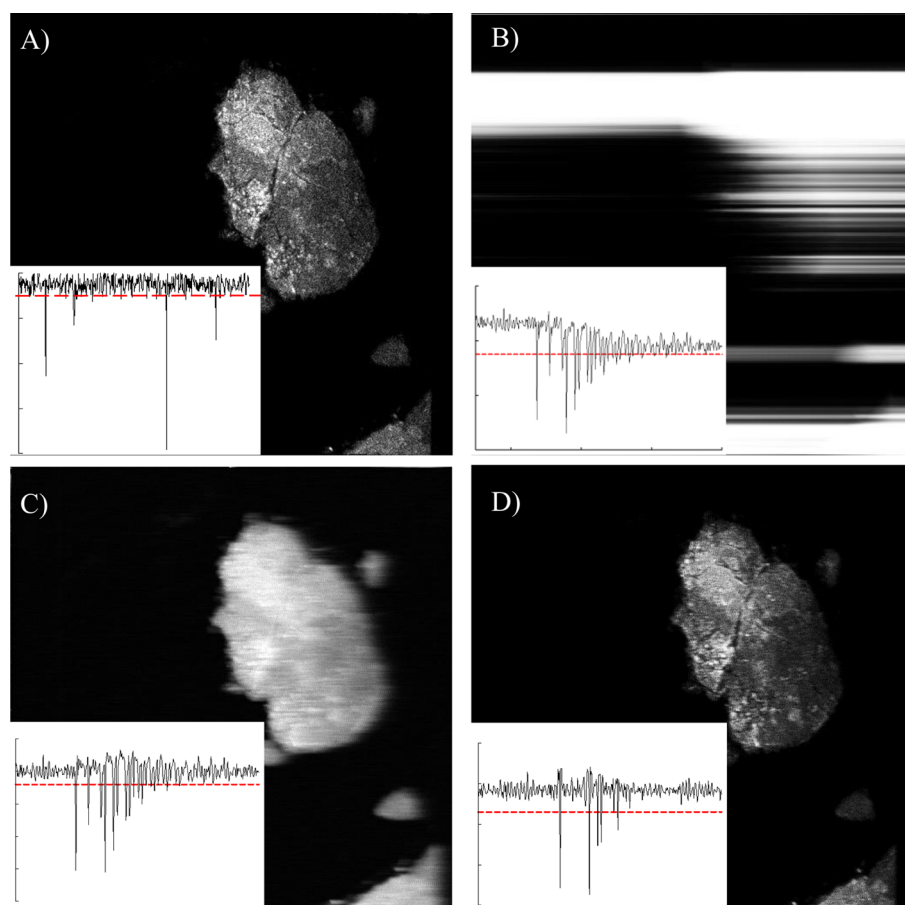
Figure 7. Two-photon excited fluorescence of tryptophan powder acquired by photon counting. (A) Micrograph acquired with an impedance-matched transmission line. Inset raw data trace. (B) Attempted photon counting from the raw impedance mismatched configuration. Inset raw data trace, with baseline drift complicating photon counting with a set discriminator threshold. (C) Photon counting of the ringing waveform following high-pass filtering to remove artifacts from baseline drift (inset data trace after high-pass filtering), and (D) photon counting following LDA-based deconvolution of the raw time-dependent data (inset data trace after high-pass filtering and LDA filtering).

the count rate by approximately 3 orders of magnitude compared to the paralysis algorithm.

TPE-UVF micrographs of tryptophan crystals are shown in Figure 7. The collected TPE-UVF light was split using a polarizing beamsplitter into two channels, one of which was terminated in 50 Ω as a reference and the other using the same 400 Ω termination design resulting in ringing. The 400 Ω channel exhibited both fast ringing and a slow drift in baseline due to capacitive charging. The drifting baseline substantially complicated the selection of a single appropriate counting threshold, resulting in highly distorted images. Application of a high-pass digital filter removed complications from baseline drift but still retained the multiple pulse ringing artifacts. From the raw images as well as the line-traces, it is clear that the artifacts produced both qualitative and quantitative errors in the measured intensity. The multiple pulses produced blurring from spreading counts across multiple pixels. Furthermore, the intensity measured in total counts is significantly biased on the basis of comparisons with the LDA-filtered image and the orthogonally polarized detection channel.

Interestingly, the output of the LDA filter consistently produced a rolling background drift over distances comparable to the length of the filter function. The origin of this baseline drift can be understood in hindsight by considering the nature of the LDA algorithm, in which the filter is designed solely to maximize the separation between coincident and noncoincident classes. The baseline drift is irrelevant to the algorithm and, therefore, is not actively corrected by the LDA filter itself. Passing the filtered data through a second high-pass filter removed the baseline offset to make the data more amenable to photon counting based on a simple threshold. Because convolution is associative, the LDA and high-pass filter can also be combined into a single digital filter by convolving the two filters with each other to further reduce computational costs, as was done prior to analysis of the images shown in Figure 7.

Not surprisingly, the act of deconvolution resulted in a reduction in the overall S/N ratio of the raw measurements, clearly indicated in the simulations shown in Figure 3. Deconvolution retains only the high frequency content within the signal capable of recovering an impulse response, which explains the significant reduction in the integrated area under each transient peak. In the analysis of simulated data, the average S/N (defined here as the peak voltage divided by the standard deviation of the background) dropped from 65 initially to 22 following deconvolution. In contrast, only a small drop in S/N was observed in the experimental measurements of the ringing waveform (S/N = 29 for the left-most peak in Figure 5 in the original data to S/N = 27 post deconvolution), presumably by nature of the greater relative signal strength at high frequencies.

Fortunately, in photon counting applications such as those considered herein, both the random noise in the baseline and noise from variance in the peak heights of the transients are naturally removed through the counting process. As a result, no significant loss in S/N in the measured counts is expected following deconvolution of photon/ion/electron counting measurements, provided the raw S/N of the measurements is sufficient to recover deconvolved transients still rising above threshold. In fact, significant improvement in the confidence of photon arrival times was observed from analysis of the deconvolved simulated data, as well as increased linear dynamic range through the removal of counting dead-time.

Along this same argument, reliable recovery of an impulse response is only expected for waveforms retaining sufficient signal content at the sampling frequency. If the impulse response removes all signal content at the highest accessible frequency, only noise is retained following deconvolution. Consequently, balance should be struck between the selection of the sampling frequency versus the S/N required for reliable photon counting postdeconvolution. Reducing the sampling frequency can potentially increase the probability of multiple photons initiated in the same sampling period. However, bias associated with such occurrences can be removed by using binomial photon counting. Because of the close relationship between the definition of the resolution and the Fisher discriminant, the value of the scalar $J(\vec{w}*)$ from combining eqs 1 and 4 may potentially be used directly to assess the sampling frequency over which reliable deconvolution may be reasonably expected.

The recovery of a deconvolved time-trace by LDA-based digital filtering was compared to two alternative strategies: nonlinear curve fitting and Richardson-Lucy digital deconvolution. Nonlinear peak-fitting of the data using standard approaches from spectroscopy and chromatography can suppress the background noise and provide the origins of overlapping peaks more accurately than digital deconvolution in most instances. However, peak fitting is an iterative procedure requiring initial guess values, complicating application for streaming data analysis. Furthermore, peak-fitting requires the *a priori* assumption of a known functional form for the peaks. Preliminary estimates based on optimized algorithms in MatLab suggest fitting times of 1.7 s per photon event for the fitting of a single ringing waveform, corresponding to approximately 5 days to process each frame in a video rate acquisition with a mean of 0.05 photons per pulse. Alternative digital deconvolution approaches were also assessed, on the basis of the iterative Richardson-Lucy deconvolution algorithm. As with many deconvolution approaches, the Richardson-Lucy algorithm requires *a priori* determination of the noise free impulse function. In general, deconvolution with the Richardson-Lucy approach recovered impulse responses with comparable or higher S/N than the LDA-based approach but at the expense of considerable additional computational time. Preliminary assessments using Matlab built-in algorithms required between 10 and 100 μs per data point on average to perform the deconvolution, corresponding to a little more than 8 s to roughly a minute per frame. While reasonable for a single frame of acquired data, the need for at least 8 s to perform the data analysis represents a significant gap to bridge relative to the 15 fps data acquisition rate. From this analysis, the long times required for nonlinear curve fitting and for iterative deconvolution using the Richardson-Lucy algorithm are incompatible with real-time data analysis at the experimental 160 MHz repetition rate for each channel.

Clearly, the improvements afforded by deconvolution must also be weighed against the computational costs associated with the data processing based on the particular application. For real-time data processing at the high data throughput rates used in this study, digital filtering arguably represents the fastest approach for performing deconvolution in terms of computational cost. Direct digital filtering for deconvolution can be performed in as little as 2 clock cycles of a field programmable gate array (FPGA) (when parallelized).[20] FPGA clock speeds in the hundreds of MHz are currently available, allowing direct real-time analysis at data throughput rates exceeding the 160 MHz acquisition rates of the present study. However, there is still an initial expense associated with the design of the appropriate digital filter. The LDA approach described herein requires significant training to reduce the noise inherent in the filter function. Provided the impulse response function does not change substantially over the time-course of a measurement as in the photon counting applications described herein, this initial investment may be easily justified by enabling subsequent high speed data analysis through simple digital filtering.

It is significant that one LDA algorithm performed reasonably well for two very different impulse response functions. No explicit models were required for treating the measurement noise or the variance in signal intensities. All of these effects were implicitly incorporated into the algorithm through the training set used to produce the LDA filters.

■ AUTHOR INFORMATION

Corresponding Author
*E-mail: gsimpson@purdue.edu.
Notes
The authors declare no competing financial interest.

■ ACKNOWLEDGMENTS

■ REFERENCES

(1) Kissick, D. J.; Muir, R. D.; Simpson, G. J. *Anal. Chem.* **2010**, *82*, 10129−10134.
(2) Muir, R. D.; Kissick, D. J.; Simpson, G. J. *Opt. Express* **2012**, *20*, 10406−10415.
(3) Sauer, M.; Hofkens, J.; Enderlein, J. Basic Principles of Fluorescence Spectroscopy. In *Handbook of Fluorescence Spectroscopy and Imaging: From Single Molecules to Ensembles*; Wiley-VCH Verlag GmbH & Co. KGaA: Weinheim, Germany, 2011.
(4) Walker, J. G. *Opt. Commun.* **2002**, *201*, 271−277.
(5) Castelletto, S. A.; Degiovanni, I. P.; Schettini, V.; Migdall, A. L. *J. Mod. Opt.* **2007**, *54*, 337−352.
(6) Wahl, M.; Rahn, H.-J.; Gregor, I.; Erdmann, R.; Enderlein, J. *Rev. Sci. Instrum.* **2007**, *78*, 033106.

(7) Finn, M. A.; Greenlees, G. W.; Hodapp, T. W.; Lewis, D. A. *Rev. Sci. Instrum.* **1988**, *59*, 2457−2459.

(8) Donovan, D. P.; Whiteway, J. A.; Carswell, A. I. *Appl. Opt.* **1993**, *32*, 6742−6753.

(9) Hillesheim, L. N.; Muller, J. D. *Biophys. J.* **2003**, *85*, 1948−1958.

(10) Bédard, G. *Proc. Phys. Soc.* **1967**, *90*, 131.

(11) Hobel, M.; Ricka, J. *Rev. Sci. Instrum.* **1994**, *65*, 2326−2336.

(12) Johnson, F. A.; Jones, R.; McLean, T. P.; Pike, E. R. *Phys. Rev. Lett.* **1966**, *16*, 589.

(13) Laundy, D.; Tang, C.; Collins, S. In Synchtron Radiation Instrumentation, *AIP Conf. Proc.*; Warwick, T., Arthur, J., Padmore, H. A., Stohr, J., Eds.; American Institute of Physics: College Park, MD, 2004; Vol. *705*, pp 977−980.

(14) Coates, P. B. *J. Phys. E: Sci. Instrum.* **1968**, *1*, 878.

(15) Abbene, L.; et al. *Med. Phys.* **2010**, *37*, 6147−6156.

(16) Gerardi, G.; Abbene, L.; La Manna, A.; Fauci, F.; Raso, G. *Nucl. Instrum. Methods Phys. Res., Sect. A* **2007**, *571*, 378−380.

(17) Riendeau, J.; et al. *IEEE Trans. Nucl. Sci.* **2008**, *55*, 40−47.

(18) Abbene, L.; Gerardi, G.; Principato, F. *Nucl. Instrum. Methods Phys. Res., Sect. A* **2013**, *730*, 124−128.

(19) Muir, R. D.; Kissick, D. J.; Simpson, G. J. *Opt. Express* **2012**, *20*, 10406−10415.

(20) Prashanth, B. U. V. *Int. J. Comp. Appl.* **2012**, *39*, 16−19.